IEEE Access
Multidisciplinary | Rapid Review | Open Access Journal

Received March 28, 2019, accepted April 15, 2019, date of publication April 23, 2019, date of current version May 3, 2019.

Digital Object Identifier 10.1109/ACCESS.2019.2912315

Advanced Drive System for DC Motor Using Multilevel DC/DC Buck Converter Circuit

ALI AHMED ADAM ISMAIL[1] AND A. ELNADY[1,2]

[1]Electrical and Computer Engineering Department, University of Sharjah, Sharjah 27272, United Arab Emirates
[2]Electrical and Computer Engineering Department (Adjunct), Royal Military College, Kingston, ON K7K 7B4, Canada

Corresponding author: Ali Ahmed Adam Ismail (aliadam999@yahoo.com)

This work was supported by the University of Sharjah for the project Design of Drive System for a Half-Model Electric Vehicle under Grant 1602040337_P and Grant 1802040393_P.

ABSTRACT This paper presents a new topology of clamped diode multilevel DC/DC buck power converter for a DC motor system. The proposed converter circuit consists of four cascaded MOSFET power switches with three clamping diodes and four voltage sources (voltage cells) connected in series. The main objective of the new topology is to reduce current ripples and torque ripples that are associated with hard switching of the traditional chopper circuit. When the voltage profile of this converter is applied on a DC motor, it positively affects the performance of the DC motor armature current and the generated dynamic torque. The output voltage of the proposed topology shows an adequate performance for tracking of reference voltage with small ripples that are normally reflected into smaller EMI noise. Moreover, it has been shown that the operation of the DC motor with the newly proposed chopper topology greatly decreases the motor armature current ripples and torque ripples by a factor equal to the number of the connected voltage cells. Both simulation and experimental results on a prototype of a DC motor are provided to validate the proposed chopper topology. The results prove that the mechanical vibration and acoustic noises have also been reduced roughly by 13 dBs with a continuous variable input voltage pattern.

INDEX TERMS Multilevel DC/DC converter, traditional DC/DC converter, and DC drive systems.

I. INTRODUCTION

Nowadays, Direct Current (DC) motors are the main horse power of the most of the industrial process operations. These motors find a wide area of applications such as robotic motions, automatic manipulations, electric and hybrid vehicles, traction system, servo systems, rolling mills, and similar applications that require adequate process. The DC motors and their associate control and drive system are classified as the first choice compared to the available Alternating Current (AC) motors and their drive systems. The DC motor acquires this popularity due to many merits such as simplicity of its control and drive system compared to AC counterpart, linear variation of the torque and speed against applied armature voltage, wide controlled speed and wide controlled torque ranges, compact of size with high power efficiency for Permanent Magnet DC (PMDC) motors, and finally the overall low cost [1]–[3].

To control the DC motor rotor position, rotor speed, or the developed torque, the motor field current or the armature voltage is controlled to achieve the control goal. The armature terminal voltage through power electronic circuits are mostly used in the motor control system especially for the relatively high-power machines [4]–[6].

The application of pulse width modulation (PWM) with a large DC link voltage to the motor windings with hard switching strategy (as the case of traditional chopper circuit) causes an unsatisfactory dynamic behavior. The abrupt variations in the voltage and the associated change in the armature current corresponding to the PWM switching initiate a wide range of voltage and current harmonics, which lead to torque ripples and the associated mechanical vibrations and acoustic noise [3], [4], [6].

The mechanical vibration and noise in electric motors have become one of the most important factors for motor selection to do a certain task [7]–[9]. The sound of the noise and the vibration in the motor are aroused mainly due to improper electromagnetic exciting forces that are continuously changed in time and space corresponding to the switching operation. This resultant variable-exciting force causes deformation in the mechanical structure and triggers the motor to vibrate [7]–[13]. These problems could be partially

The associate editor coordinating the review of this manuscript and approving it for publication was Yijie Wang.

solved by LC filters that smoothen the output voltage of the chopper, which applies the required voltage in accordance with the load torque demand. However, when fast dynamic torque response is required, especially with heavy armature current machines, it will be very difficult to achieve the required demand through LC filters.

Although many researchers have studied the source of sound noise and have described the modelling and predictions of vibration and noise in permanent motors [8]–[12], few research works have been exerted to reduce the noise and vibration in these motors. In [7], Hong *et al.* present a method where a copper ring has been fixed on the permanent magnet pole of the brush DC motor to reduce the mechanical vibration, this method shows successful reduction in vibration due manufacturing improperness. Another important research work has been carried out to reduce noise and vibration due to the PWM applied on induction motors [12], where a new switching frequency is proposed to decrease the noise level and losses. This method succeeds to reduce the noise level by 5 dB during starting and general up to 15 dBs reduction has been observed. Many other relevant publications have partially addressed the problem with special focus on the performance of the DC motor control algorithms [5], [4] [13]–[27]. In [13], an observer based nonlinear controller to deal with cogging torque disturbances in permanent magnet DC motor has been presented. The authors succeed to reduce tracking errors due cogging torque. However, the presented results show high armature current ripples which lead to torque ripples and acoustic noises. In [14], a new DC/DC converter has been developed to be used with an energy storage system for electric vehicles. The structure of the developed method in [14] is composed of two voltage sources, the result of this method gives improved efficiency; however, this method does not solve exactly the problems of current and torque ripples in motor performance profile. In [15], the researchers have presented an algebraic approach for fast feed-forward adaptation of the angular velocity trajectory tracking task in a boost-converter driven DC- motor system. The same researchers have successfully estimated the load torque perturbations using the noisy measurements of the state variables. In [16], the authors have presented detailed information for the control and design of the buck converter driving DC motor. Sira-Ramirez *et al.* [16] have provided a comparative study to test the performance of many different controllers. They have presented a Lyapunov stability analysis to design a DC/DC chopper circuit for DC motor. The objective of their design is to control the current/torque and to tune speed of the motor for industrial applications. In [4], [17], [18], the much effort has been directed towards the design of smooth starter for a DC/DC buck converter for a DC motor. In these publications, some means of flatness control and hierarchical control of some controllers such as sliding mode and PI controllers are developed to directly control the rotor speed or to reject disturbances [17]. The problem of uncertainties, disturbances and nonlinearities of DC motor parameters when powered by DC/DC power converters normally leads to torque and current pulses that need to be compensated. Some papers, [20]–[24], have tackled these problems either with fuzzy logic/neural network control system [20], [21], or with adaptive robust control with extended state observer [22], or with passivity-based control algorithm that utilizes buck boost converters [23], or with singular perturbation technique of controller design to solve the problem of uncertainties for DC motor equipped by multi-level DC-DC converter [24].

This paper proposes a new Multilevel Converter Circuit (MLCC) for the DC motor drive system to achieve fast dynamic torque performance with reduced vibration. Unlike the existing neutral point clamped diode topologies [25], the developed method separate the multilevel stage from the H-bridge, which reduces the number of switching elements for the converters with levels greater than four. The developed method guarantees small current and torque ripples as well as reduced hazards of switching large voltage across the power switches. The proposed MLCC divides the input voltage into many levels and keeps switching between two adjacent levels to achieve better tracking for the reference voltage.

II. THE PROPOSED MULTILEVEL CHOPPER STRUCTURE

The proposed block diagram of the multilevel chopper circuit (MLCC) for a DC motor drive system is shown in Fig. 1. This suggested system consists of the proposed MLCC block, H-bridge block in order to control the direction of the motor rotation, PMDC motor, in addition to many control blocks that arrange and synchronize the operation of the whole system.

In this research work, the suggested multilevel chopper circuit (MLCC) is a 5-level power converter as illustrated in Fig. 2, it is composed of four controllable power switches such as power MOSFET. The MLCC consists of three clamped diodes, (D_1, D_2 D_3), preferably Schottky diodes and freewheeling diode $D_{F.}$ These diodes together with the power switches actualize the correct operation of the multilevel chopper circuit.

The voltage of the sources V_{DC1}, V_{DC2}, V_{DC3} and V_{DC4} are of equal or different voltage values. These independent DC voltage sources could be cell storage batteries, solar cell units or any equivalent DC voltage sources.

The suggested switching signals applied to the MLCC to obtain the 5-level voltage values at the output terminals of the converter can be arranged as given in Table 1.

TABLE 1. Switching signal and resulted voltage ranges.

Switching state Q_1 Q_2 Q_3 Q_4	Voltage Level code	DC Standard Voltage value
0 0 0 0	V0	0
1 0 0 0	V8	V_{DC1}
1 1 0 0	V12	V_{DC1}+ V_{DC2}
1 1 1 0	V14	V_{DC1}+ V_{DC2}+V_{DC3}
1 1 1 1	V15	V_{DC1}+ V_{DC2}+V_{DC3}+V_{DC4}

The voltage value between any two voltage levels can be obtained by a step-down chopper mode between that voltage levels. For example, if a nonstandard voltage level V_x must be

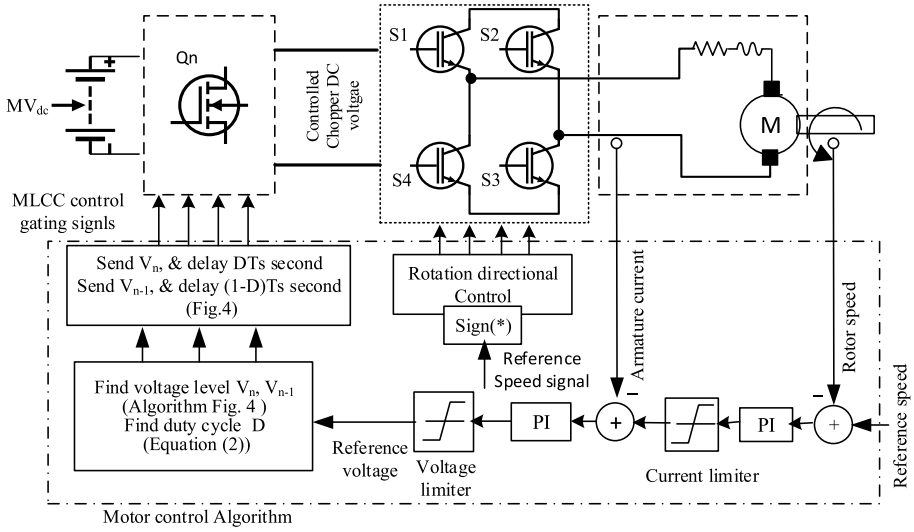

FIGURE 1. Block diagram of MLCC driving a DC motor.

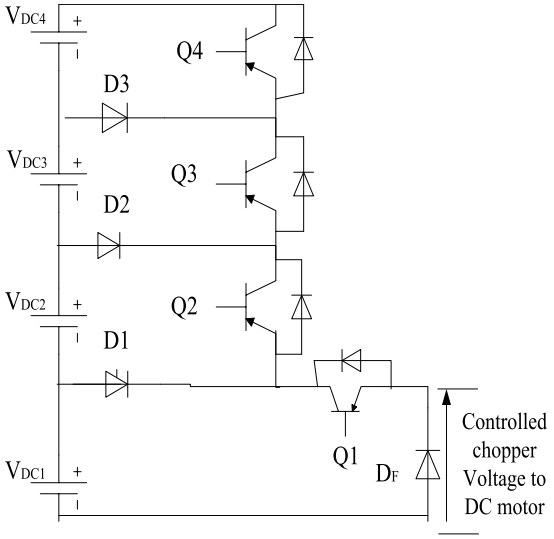

FIGURE 2. Configuration of 5-level diode clamped multilevel chopper circuit (MLCC).

obtained at sampling instant "k", the algorithm determines the voltage ranges of V_x in the first stage as shown in Fig.3:

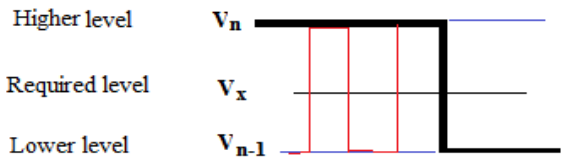

FIGURE 3. Range limits of the required voltage V_x.

Once the required voltage level V_x is determined between V_n (higher voltage level) and V_{n-1} (lower voltage level), the average voltage $V_x$can be calculated at sampling instant "k " as:

$$V_x = \frac{T_s D(k) V_n + T_s(1 - D(k)) V_{n-1}}{T_s} \tag{1}$$

where:

T_s is the sampling period

D is the per unit duty cycle

DT_s is the switching ON time of V_n, with V_{n-1} OFF

$(1\text{-}D)T_s$ is the switching ON time of V_{n-1}, with V_n OFF

Using (1), the duty cycle at sampling instant k is determined as:

$$D(k) = \frac{V_x - V_{n-1}}{V_n - V_{n-1}} \tag{2}$$

In order to have V_x, the voltage level V_n is switched ON for DT_s seconds followed by switching ON of V_{n-1} for $(1\text{-}D)T_s$ seconds. A flow chart showing possible switching algorithm for the proposed topology is shown Fig. 4.

III. ELECTRIC ANALYSIS OF THE MLCC-DC MOTOR SYSTEM

It is assumed that there is a permanent magnet DC (PMDC) motor with constant field excitation and unidirectional of rotation, the electrical equivalent circuit of the MLCC driving a DC motor (*the control system is not shown*) can be drawn as given in Fig. 5.

Consider the MLCC equations as given in section 2, the PMDC motor dynamic equations for the circuit in Fig. 5 can be written as:

$$\left.\begin{aligned} V_{in} &= E_a + R_a i_a + L_a \tfrac{di_a}{dt} \\ E_a &= K_g \omega \\ T_e &= J \tfrac{d\omega}{dt} + B\omega + T_L \\ T_e &= K_t i_a;\ K_t = K_g \end{aligned}\right\} \tag{3}$$

where V_{in} is the applied DC voltage pattern from the MLCC; E_a is the DC motor counter back generated voltage; K_g and K_t

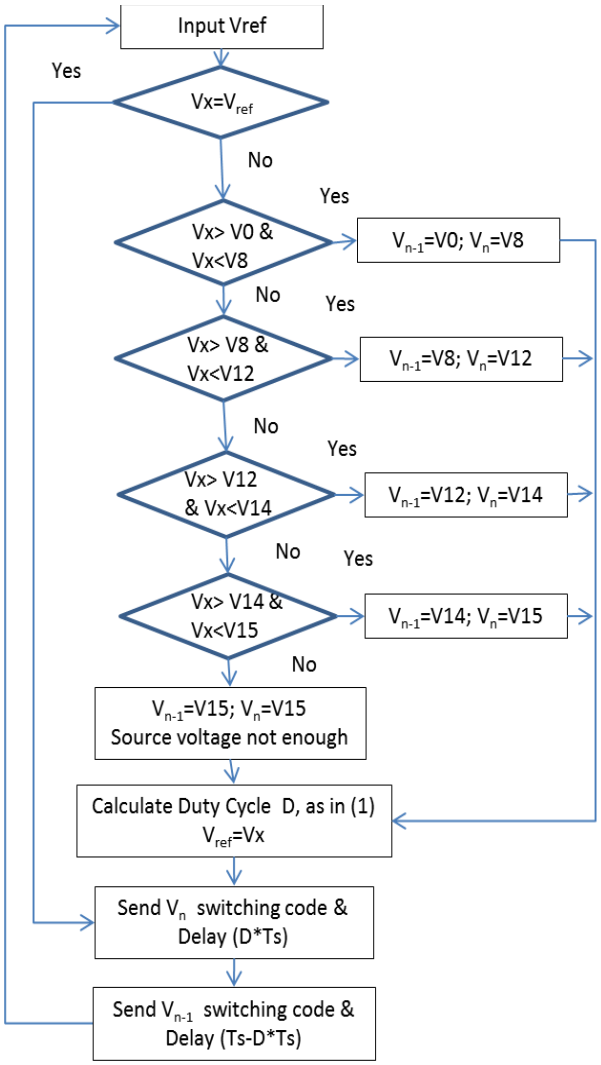

FIGURE 4. Control algorithm chart of the proposed MLCC.

are the generated voltage and the motor developed torque constants. The T_e and T_L are the motor developed torque and the motor load torque, respectively, ω is the rotor angular speed in rad/s, J is the inertia constant, β is friction constant, L_a and R_a are the armature winding resistance and inductance, respectively.

If all power switches Q_1-Q_M are assumed ideal and the Schottky clamped diodes are also ideal, the above circuit can be redrawn as lumped circuit as shown in Fig. 6. The operating modes of this equivalent circuit can be restricted to three switching modes, two of these modes are engaged to the two input lumped voltage sources nV_{DC} and $(n\text{-}1)V_{DC}$ and the third mode represents the operation through the freewheeling diodes D_F.

Assume clockwise direction of rotation, the MLCC-DC motor system equations through the different operating modes corresponding to the equivalent circuit given in Fig. 6 can be expressed as follows:

Mode 1: This mode is defined by the time period $[0\text{-}DT_s]$, when the power switches are in the S_{High} position; with n series connected controllable switches are simultaneously in ON position. The system equations are as follows:

$$\left.\begin{aligned}\frac{di_a}{dt} &= -\frac{R_a}{L_a}i_a - \frac{K_g}{L_a}\omega + \frac{nV_{DC}}{L_a}\\ \frac{d\omega}{dt} &= \frac{K_g}{J}i_a - \frac{B}{J}\omega - \frac{T_L}{J}\end{aligned}\right\};\ 0 \le t \le DT_s \qquad (4)$$

Mode 2: This mode is transition mode; it defines the transient period that starts when the switch is disconnected from the S_{High} position and ends when the switch is connected to the S_{LOW} position, i.e. just before the low voltage level $(n\text{-}1)V_{DC}$ comes into effect. This transition period, normally very small, depends on the switching time of the power switches. In this mode, the motor current flows through the freewheeling diode D_F, and the system equations can be written as,

$$\left.\begin{aligned}\frac{di_a}{dt} &= -\frac{R_a}{L_a}i_a - \frac{K_g}{L_a}\omega\\ \frac{d\omega}{dt} &= \frac{K_g}{J}i_a - \frac{B}{J}\omega - \frac{T_L}{J}\end{aligned}\right\};\ DT_s \le t \le DT_s + (t_{off} + t_{on}) \qquad (5)$$

where $(t_{off} + t_{on})$ is the transition period; t_{off} is switching OFF time and t_{on} is the switching ON time of the

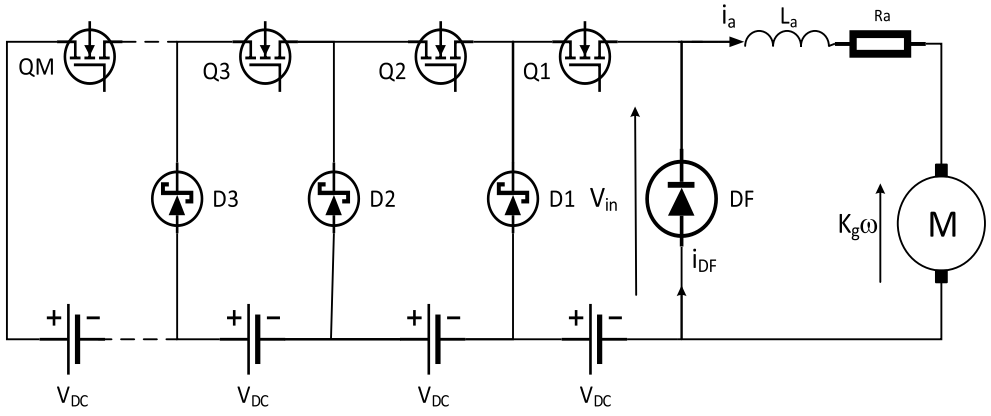

FIGURE 5. MLCC driving a DC motor.

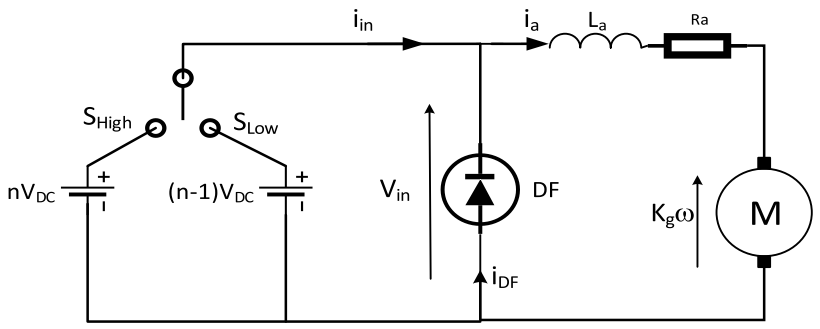

FIGURE 6. Simplified lumped equivalent circuit of the MLCC-DC motor system.

power switches. Typical values for this transition time are 0.1-0.15 microsecond for the power MOSFET **IRFP460**. During this period the motor current, the motor speed, the generated counter voltage E_a, and the motor developed torque are slightly decreased. The reduction in the values of these variables continue until the switch S_{Low} comes into operation and the mode transfers to mode 3.

Mode 3: This mode represents the case when the power switch is in the S_{Low} position; where *(n-1)* series connected switches are simultaneously in ON-position during the time period $[DT_s + (t_{on} + t_{off})]$-$Ts$. The system equations are as follows:

$$\left.\begin{aligned}\frac{di_a}{dt} &= -\frac{R_a}{L_a}i_a - \frac{K_g}{L_a}\omega + \frac{(n-1)V_{DC}}{L_a}\\ \frac{d\omega}{dt} &= \frac{K_g}{J}i_a - \frac{B}{J}\omega - \frac{T_L}{J}\end{aligned}\right\};\ DT_s + t_{on} + t_{off} \le t \le T_s \tag{6}$$

For the permanent magnet DC motor, the motor developed torque T_e is linearly proportion to the armature current i_a. Hence it is enough to select armature current and rotor speed as state variables to fully describe the system state-space behavior. Additionally, for a moderate switching frequency less than 10 kHz ($T_s \ge 100\mu S$); the effect of $(t_{on} + t_{off})$ is negligibly small on the system state variables, so it can simply be excluded from the averaging result during one sampling time, and the overall averaging state-space model can be written as,

$$\begin{bmatrix}\frac{di_a}{dt}\\ \frac{d\omega}{dt}\end{bmatrix} = \begin{bmatrix}-\frac{R_a}{L_a} & -\frac{K_g}{L_a}\\ \frac{K_g}{J} & -\frac{B}{J}\end{bmatrix}\begin{bmatrix}i_a\\ \omega\end{bmatrix} + \begin{bmatrix}\frac{(n-1)(1-D)+nD}{L_a} & 0\\ 0 & -\frac{1}{J}\end{bmatrix}\begin{bmatrix}V_{DC}\\ T_L\end{bmatrix} \tag{7}$$

The above equation is a time-invariant system that describes the behavior of the motor. The duty cycle D can be considered constant and V_{DC} as an input variable, equally can be considered as a variable as a function of time $D(t)$ while V_{DC} is constant. The frequency domain solution of equation (7) can be written as:

$$\begin{aligned}I_a(s) &= \frac{(\tau_m s+1)[n-1+D)]V_{DC}(s)/R_a}{\tau_m\tau_a s^2 + (\tau_m+\tau_a)s + 1 + k_g^2/R_a\beta}\\ &\quad - \frac{J^2 k_g/R\beta}{\tau_m\tau_a s^2 + (\tau_m+\tau_a)s + 1 + k_g^2/R_a\beta}T_L(s)\\ \omega(s) &= \frac{k_g/\beta}{(\tau_m s+1)}I_a(s) - \frac{1/\beta}{(\tau_m s+1)}T_L(s)\end{aligned} \tag{8}$$

where $\tau_m = J/B$ and $\tau_a = L_a/R_a$ are the mechanical time constant and the electrical time constant, respectively.

In the proposed MLCC system, the converter switching is restricted between two voltage levels {nV_{DC} and (n-1)V_{DC}}, hence the maximum change in the motor input dynamic voltage is only 1 cell voltage level (V_{DC}) and varies with the variation of the duty cycle. Assume that the load torque is constant (*i.e.* $T_L(s)=0$), and consider the duty cycle $D(t)$ as input variable with constant value of voltage V_{DC}, and knowing that the lower level of the input voltage (n-1)V_{DC} in equation (8) produces no change in the system dynamic, the above system of equation can be used to obtain the system dynamic change using the following equations:

$$\begin{aligned}I_a(s) &= \frac{(\tau_m s+1)V_{DC}/R_a}{\tau_m\tau_a s^2 + (\tau_m+\tau_a)s + 1 + k_g^2/R_a\beta}D(s)\\ \omega(s) &= \frac{k_g V_{dc}/R_a\beta}{\tau_m\tau_a s^2 + (\tau_m+\tau_a)s + 1 + k_g^2/R_a\beta}D(s)\end{aligned} \tag{9}$$

From (9), it can be concluded that the current ripples and the speed ripples can be effectively reduced by reducing the variation of the applied DC voltage during the chopper ON and chopper OFF periods.

IV. SIMULATION RESULTS

To evaluate the performance of the proposed multilevel chopper circuit, two Simulink models are built. One model is given for the proposed MLCC with the structure given in section II and the other one is given for the traditional chopper circuit with one fixed DC voltage source and one controllable switching element. The traditional chopper circuit works in a step-down mode to achieve the required reference voltage. The results of the output voltage performance is shown

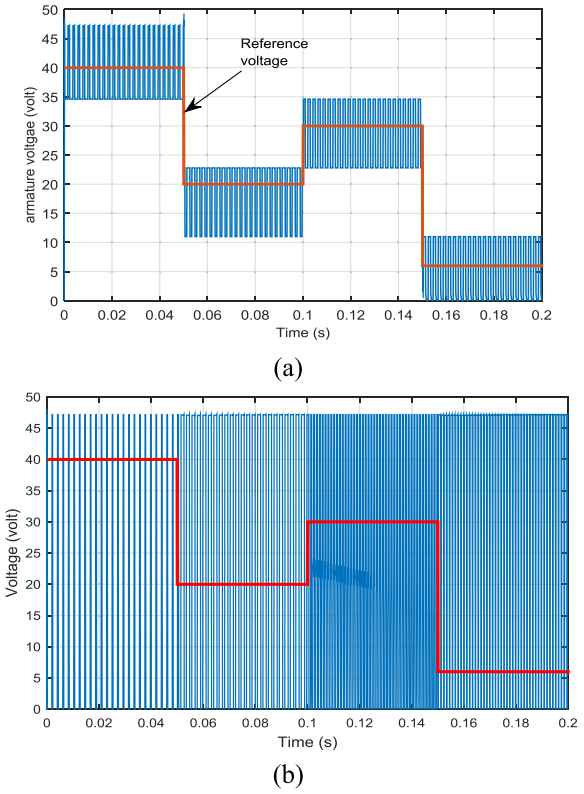

FIGURE 7. Chopper circuit output voltage, (a): The proposed MLCC, (b): Tradition hard switching chopper.

in Fig. 7, where the reference voltage (red) is changed from 40V to 20V then to 30V and thereafter to 6V for a duration of 0.05 s for each voltage level. It is clear from the comparison of these two figures that the proposed system works properly to provide the required level voltage to the load. The system keeps switching only between two consecutive voltage levels, while the tradition system of Fig. 7b must follow hard switching across the ultimate voltage range (0-48V) to provide the required reference voltage.

One typical application of the proposed MLCC is in the field of electrical vehicles that are mostly operated by DC motors. These types of vehicles work in an open control mode, where the applied voltage level to the armature of the DC motor determines the vehicle speed (or the driving torque). The voltage source, in such vehicles, is composed of 4 batteries (each of 12 volts connected in series), which provide typical voltage requirements for the proposed MLCC. Thus, the performance of the proposed MLCC is simulated with such a typical PMDC motor whose specifications are given in Table 2. The results of the simulation with an open control mode are shown in Fig.8 to Fig.12.

In Fig.8-Fig.10, the soft starting of the PMDC at no- load has been tested by applying a voltage level structure of 35V-40V-45V with time ranges of 0.5s for each voltage level to the motor terminals. From these figures, the smooth starting speed performance and its corresponding torque and armature

TABLE 2. PMDC motor specfications used for simulation.

Parameter	Value
Rated power	3.02 kW
Rated torque	4.35 Nm
Rated speed	6724 rpm
Rated voltage	48 V
Rated current	75A
Ra	0.48 Ohm
La	1.4 mH
J	0.0117
B	0
Km	0.0631 Nm/A
Kg	1/138 V/rpm

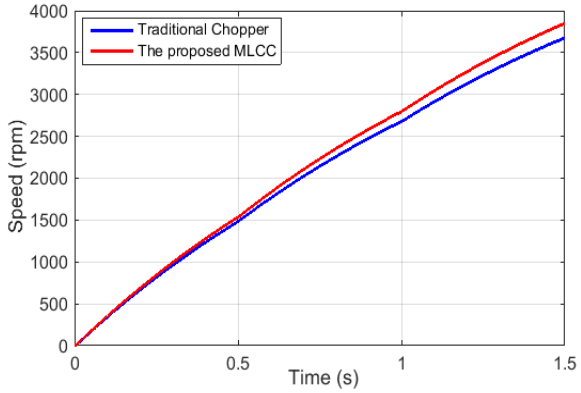

FIGURE 8. Smooth starting speed performance of the PMDC motor, the proposed MLCC (in red) and Traditional chopper drive (in blue).

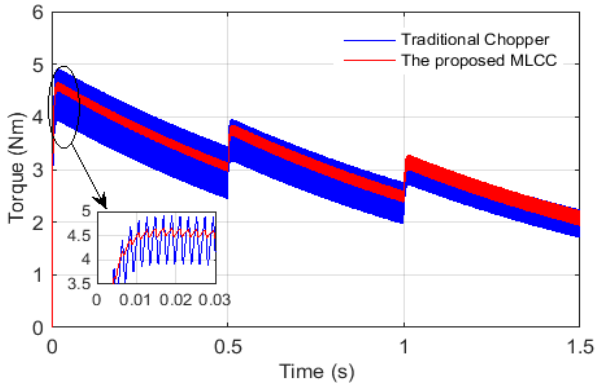

FIGURE 9. Smooth starting developed torque of the PMDC motor, the proposed MLCC (in red) and Traditional chopper drive (in blue).

current have been observed as compared to the traditional chopper drive. The buildup speed perfomance in Fig. 8 shows almost the same continously increasing speed with a considerable fast response in the case of the proposed MLCC.

The soft starting torque and the coresponding armature current, shown in Fig. 9 and Fig.10 respectively, illustrate the meritorous performance of the proposed MLCC in terms

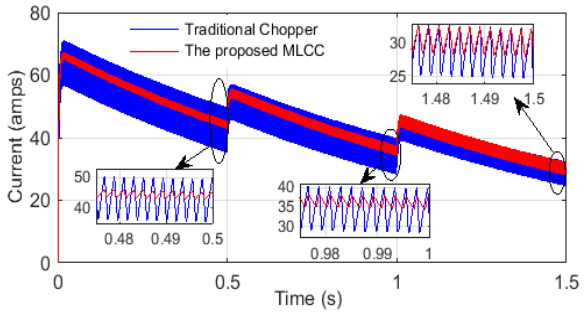

FIGURE 10. Smooth starting armature current of the PMDC motor, the proposed MLCC (in red), and Traditional chopper drive (in blue).

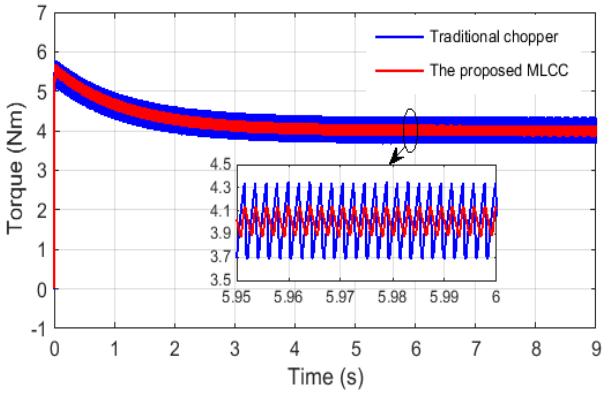

FIGURE 11. Torque performance with 4 Nm connected to the motor shaft, the proposed MLCC (in red), and Traditional chopper (in blue).

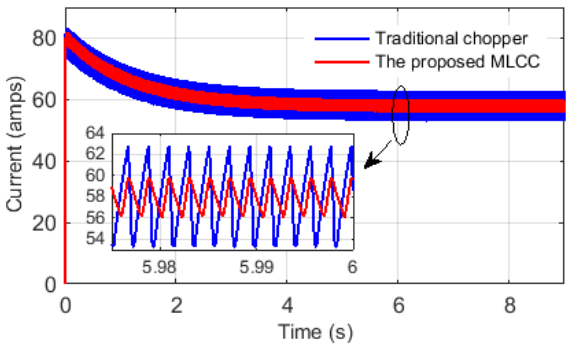

FIGURE 12. Armature current performance with 4 Nm connected to the motor shaft, the proposed MLCC (in red), and Traditional chopper (in blue).

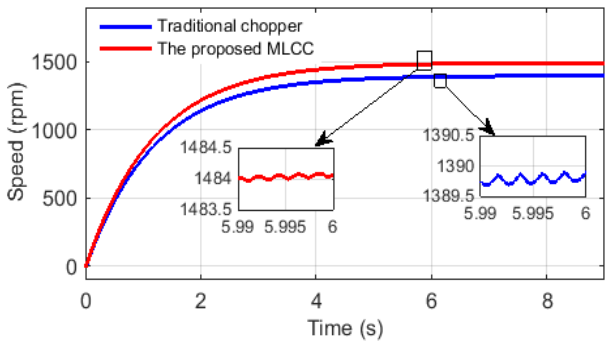

FIGURE 13. Steady state speed performance with 4 Nm connected to the motor shaft, the proposed MLCC (in red), and Traditional chopper (in blue).

of the current ripples, torque ripples as well as the overall average armature current requirements.

Although the traditional chopper circuit provides apparentlly higher starting torque (4.95 Nm) than the proposed MLCC (4.6 Nm), it is also associated with a high starting current of 76A while that of the proposed MLCC is 68A. This higher starting current in presence of higher current ripples result in a mechanical vibration and sound noise during the soft starting of the motor.

The operation of the motor at starting and steady-state performance with 40 V applied armature voltage and 4.0 Nm load torque is simulated for the both drive systems (proposed and traditional ones) under the same operating conditions. The motor torque, the armature current and speed profile responses for the proposed MLCC system compared to the traditional hard swtiching chopper system are given in Fig. 11, Fig.12, and Fig 13, respectively.

The motor starting torque in Fig. 11 shows that the proposed MLCC provides a slightly lower starting torque with smaller torque pulses, while the traditional chopper drive system provides a high starting torque with high torque pulses (as can be inferred from the thickness of the torque pulsation) due to hard voltage switching. These high pulses result in jerky starting of the motor and sharp starting sound noise as the case without load in Fig. 9.

The torque ripple in the steady-state performance is shown in the magnified part of Fig.11 for the both drive systems. The peak to peak torque ripple is approximately 0.7 Nm for the traditional chopper drive circuit and around 0.2 Nm for the proposed MLCC. It can be roughly concluded that with the proposed MLCC, the torque ripple is decreased by a factor of n (equal to the number of the DC voltage source cells). This reduction in the torque ripples eventually reflects on less noise and reduced mechanical vibration. In addition, the armature current in Fig.12, which is like the developed torque performance, shows smaller current ripples for the proposed MLCC. These smaller ripples lead to less ohmic losses, and less harmonics and low EMI noise. The corresponding speed profile in Fig.13 shows that for the same applied average voltage, the proposed MLCC gives a relatively higher speed level. In addition, the magnified part of the Fig.13 shows that the speed pulsation is higher in the case of the traditional chopper.

To accurately evaluate the proposed topology, the MLCC is simulated in closed loop control mode. The simulated circuit is arranged as given in Fig.1. The tuned parameters of the current loop controller are ($K_i = 0.2$ and $K_p = 2$, and high voltage limits of 48V), and that of the speed controller are ($K_i = 16$ and $K_p = 1.6$, and current limit of 90 amps). The speed reference is changed from initial value of 100 rad/s to

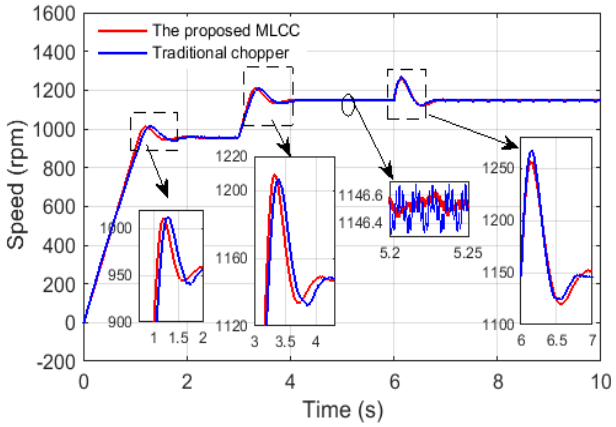

FIGURE 14. Closed loop speed control: Speed performance, the proposed MLCC (in red), and traditional chopper (in blue).

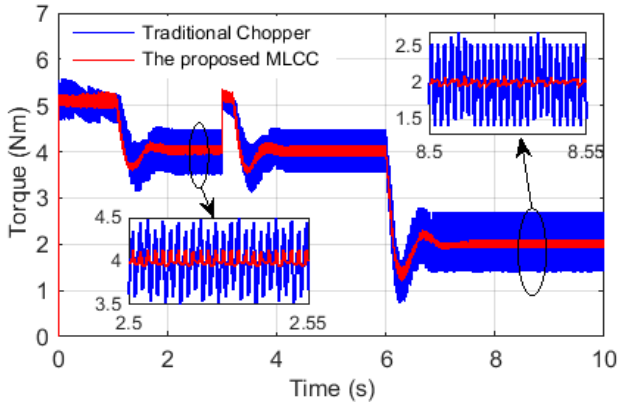

FIGURE 15. Closed loop speed control: Torque performance, the proposed MLCC (in red), and Traditional chopper (in blue).

120 rad /s or (*in rpm as 100∗60/2∗π to 120∗60/2∗π*) at time t= 3 second. The load torque is changed from an initial value of 4 Nm to a final value of 2 Nm at time t = 6 second.

The detailed speed and torque performances are shown in Fig. 14 and Fig. 15 respectively. The controlled speed performance for the both methods (*the proposed in red and the traditional in blue*) shows almost the same general performance at starting and at steady state. However, the magnified parts of the Fig.14 show that the proposed MLCC has smaller speed ripples and relatively smaller overshoot during the load change at time = 6 second. On the other hand, the corresponding torque profile shows an outstanding performance of the proposed MLCC as can be seen in the magnified parts of the Fig.15. Although the average dynamic time response is almost the same, the torque overshoot at load torque change point is higher than the proposed MLCC, in addition the torque ripples of the traditional chopper circuit are extremely high.

V. EXPERIMENTAL RESULTS

To validate the operation of the proposed DC/DC chopper topology, the experimental platform shown in Fig.16 is

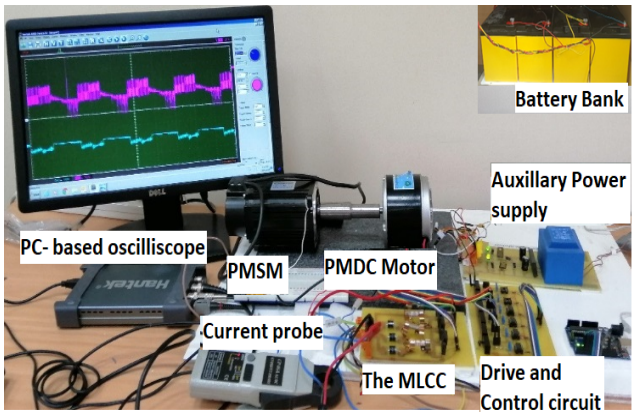

FIGURE 16. The setup of the proposed MLCC-DC motor system.

arranged to study the practical performance of the multilevel converter. The setup comprises of a permanent magnet DC motor (PMDC) with specifications given in Table 3. The PMDC motor is coupled to a permanent magnet synchronous machine (PMSM) that is operated as a generator to load the DC motor. The setup also includes the proposed multilevel chopper circuit that has been built with power MOSFET transistors (IRFP460) as controlled power switches and clamped diodes (P600k). The drive circuit of the chopper circuit is realized through a microcontroller and an opto-isolator system working at 1kHz switching frequency. The control system accepts the input voltage command signals to determine the output switching signal pattern to the chopper gate signals. The input voltages (voltage cells) applied to the converter are four DC batteries (RAYTON 12V, 100AH).

TABLE 3. Specfications of the PMDC motor used in experimental work.

Parameter	Value
Rated power	300W
Rated speed	540/1080 rpm, no of poles=4
Rated voltage	12/24 V
Rated current	12.5A
Ra	1.3 Ohm
La	1.08 mH
J	$0.24x10^{-3}$
B	0
K_g	0.013 V/rpm or 0.22037 rad/s

Two chopper circuit have been set for the experimental results. One for the traditional chopper circuit with only one switching element and one voltage source of 48V (4 batteries in series), and the other for the proposed multilevel converter with four power switches and four voltage cells each of 12 volts clamped to the power switches. The measurements of the voltages, currents, and acoustic noise with and without freewheeling diodes have been observed as depicted from Fig.17 to Fig. 21.

To validate the voltage output operation pattern of the proposed MLCC, a voltage reference pattern of this sequence

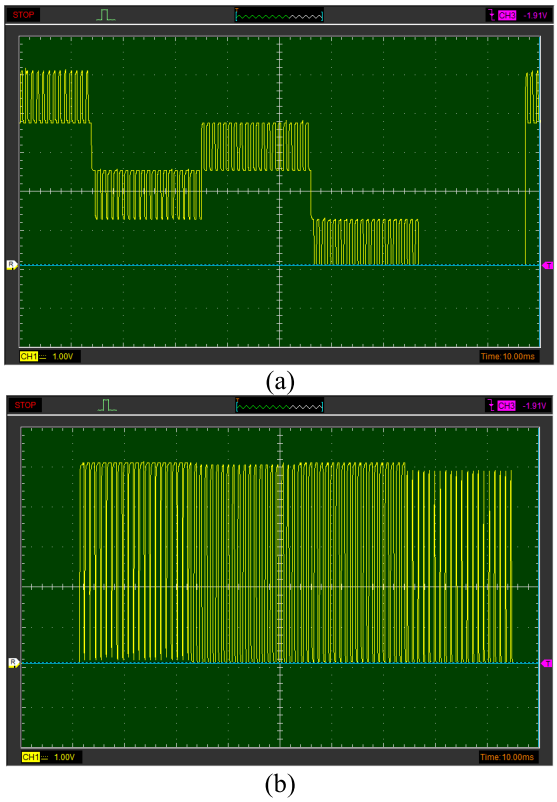

FIGURE 17. Chopper output voltage responses for input pattern of 40V→ 20V→ 30V→ 6V, 10V/div, (a): the proposed MLCC, (b): the traditional chopper circuit.

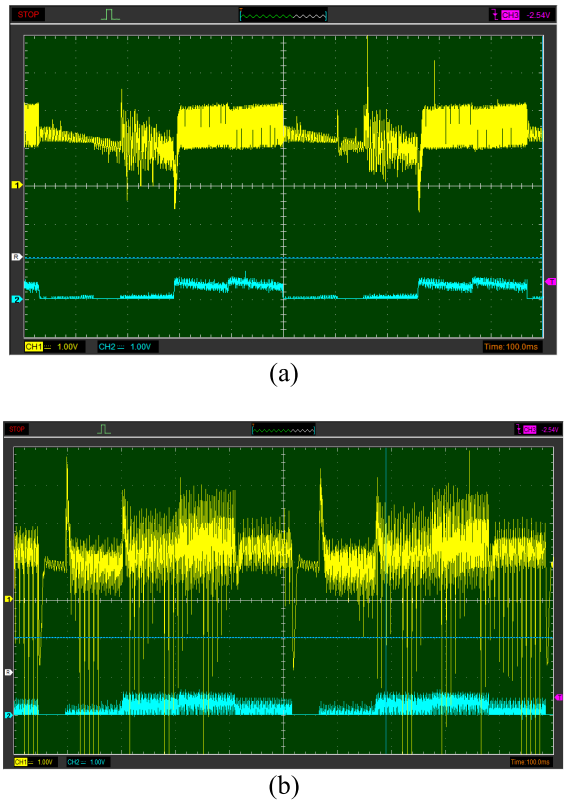

FIGURE 18. Voltage (upper), 20 V/div and torque/current, 8A/div (lower) response of PMDC motor without freewheeling diode, (a): the proposed MLCC, (b): the traditional chopper circuit.

40V→ 20V→ 30V→ 6V with a duration of 0.05s for each voltage level has been applied to both the traditional chopper circuit with a constant input voltage of 48 V and to the proposed MLCC. The chopper output voltage of the two systems (the traditional and proposed ones) are shown in Fig. 17. It can be seen that the proposed converter circuit in Fig. 17-a adequately follows the reference voltage pattern mentioned above with the minmium voltage pulses. These pulses are limited to the maximum of one cell voltage (12V). On the other hand, the traditional chopper cricuit gives the same average output voltage with a large voltage pulses of 48 V (4 cells) due to hard swiching strategy. It is worth noting that the result in Fig.17 matches with the corresponding simulated result in Fig. 7.

The motor dynamic response is tested for the input sequence voltage pattern of 6V→ 16V→ 20V→ 12V with a duration of 0.1s for each voltage level. Only two cells of the input voltage are used to not exceed the DC motor limit values. The sequence voltage pattern is applied to the motor-chopper system with and without freewheeling diode across the motor terminals. The armature current (representing developed torque) and terminal voltage performance of the motor are shown in Fig. 18 and Fig. 19 for the proposed MLCC-DC motor system and the traditional chopper-DC motor system, respectively.

As can be seen in Fig. 18, the performance of the developed torque and motor terminal voltage of the proposed MLCC follows the applied reference voltage pattern adequately with the minimum voltage ripples and torque ripples, while the response of the traditional chopper circuits is full of voltage ripples and torque ripples. The average torque ripples ratio between the MLCC response/Traditional Chopper response varies between 0.2 up to 0.5 depending on the applied voltage level. This reduction in the torque ripple is reflected on the reduction of the measured motor acoustic noise and vibration from 68 dBs for the tradition chopper –DC motor system down to 55 dBs for the proposed MLCC-DC motor system.

The torque or armature current ripples in the traditional system is mainly due to hard switching strategy of the power switches that produce an abrupt variation in the voltage and current of the motor [7], [9]. However, with the proposed MLCC, this hard switching is limited to only one cell voltage level, which reduces the torque ripples by a factor of n (n is the number of the converter cells).

The freewheeling diode affects the operation of the two systems, (traditional and proposed ones), as depicted in Fig.19. It is clear that the freewheeling diode highly influences the voltage pattern for both systems that are normally distorted due to the inductance of the armature circuit ‘‘La’’. Bearing in mind, this effect is small in the case of the proposed MLCC-DC motor system due to direct switching

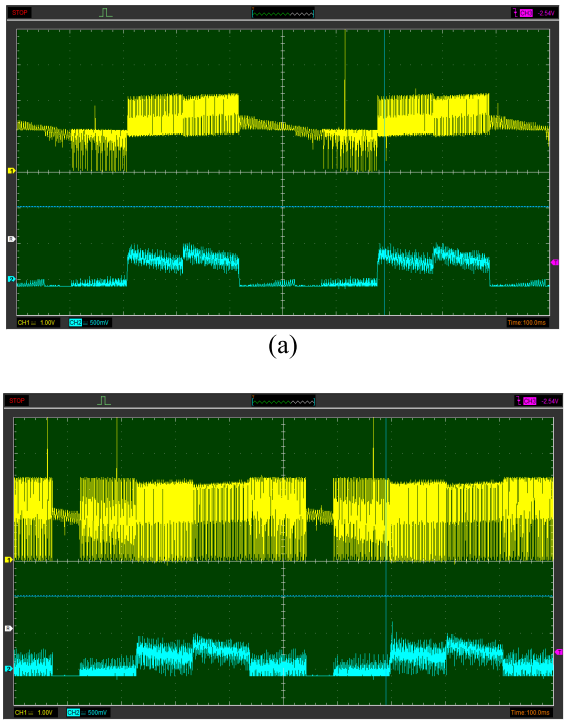

FIGURE 19. Voltage (upper), 20 V/div and torque/current, 4A/div (lower) response of PMDC motor with freewheeling diode, (a): the proposed MLCC, (b): the traditional chopper circuit.

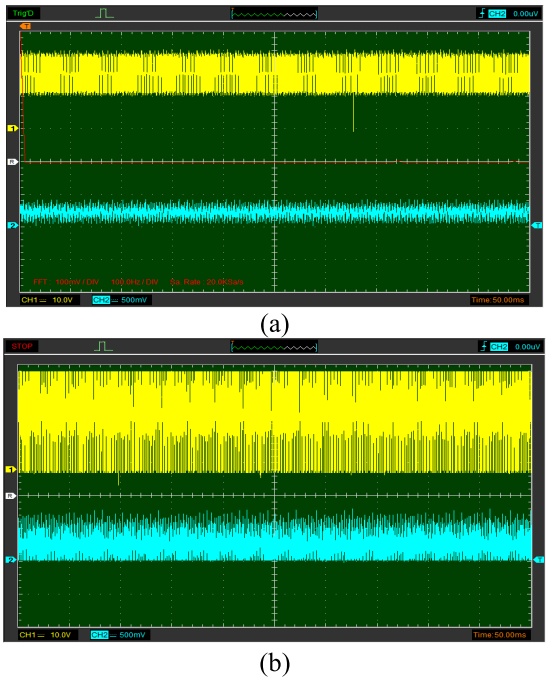

FIGURE 20. Steady state voltage (upper), 10V/div and current (lower), 4A/div, (a): the proposed MLCC, (b): the traditional chopper circuit.

between two consecutive voltage levels. This effect gets smaller if the switching frequency is increased.

To study the performance of the motor at steady state, the PMDC is operated with 18V input voltage from the two

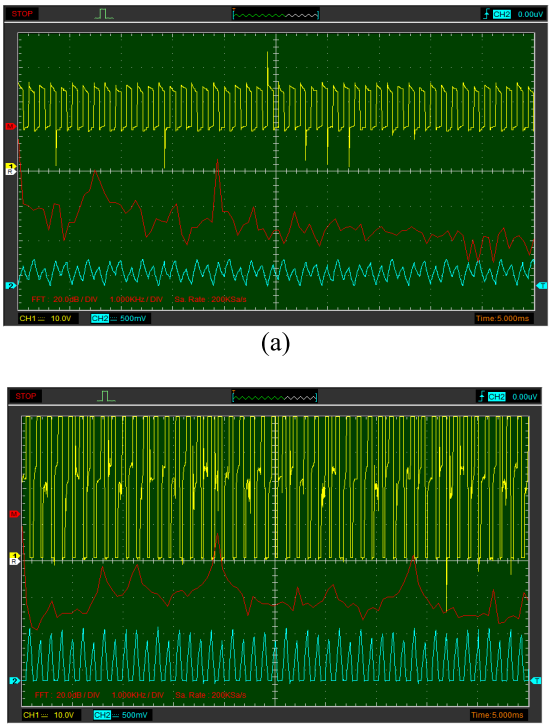

FIGURE 21. Steady state applied voltage (upper), 10V/div and current ripples (lower), 4A/div and current noise in dBs (in red), (a): the proposed MLCC, (b): the traditional chopper circuit.

TABLE 4. Quantitative summary of the ripple and noise reduction.

Parameter for Comparison	Traditional Chopper	Proposed MLCC	Reduction level
Voltage ripple (volt)	39	13	66%
Current ripple (amps)	5.6	2.4	57%
Current harmonic noise (dBs)	-63	-46	20 dBs
Acoustic noise level (dBs)	67	59	8 dBs

converter systems (the traditional and proposed ones). The steady state applied voltage and armature current are displayed in Fig. 20, while the current/torque ripples and current noise in dBs are depicted in Fig. 21. Accurate inspection of these figures shows that the current ripples of the MLCC is 2.4 A (peak-peak) while that of the traditional chopper drive is 5.6 A (peak to peak). The current harmonics and noise level obtained from Fast Fourier tool (in red in Fig.21) proves that the relatively higher noise level is generated from the traditional chopper drive system. These harmonics lead to high vibration and sound levels as depicted in Fig. 22 with 59 dBs for the MLCC system and 67 dBs for the traditional chopper circuit.

Table 4 summarizes the quantitative experimental performance of the proposed MLCC in ripple and noise reduction during steady state as compared to the traditional chopper circuit.

It can be observed from the simulation results and the experimental result and summary in Table 4, that the proposed MLCC can effectively reduce the torque ripples and

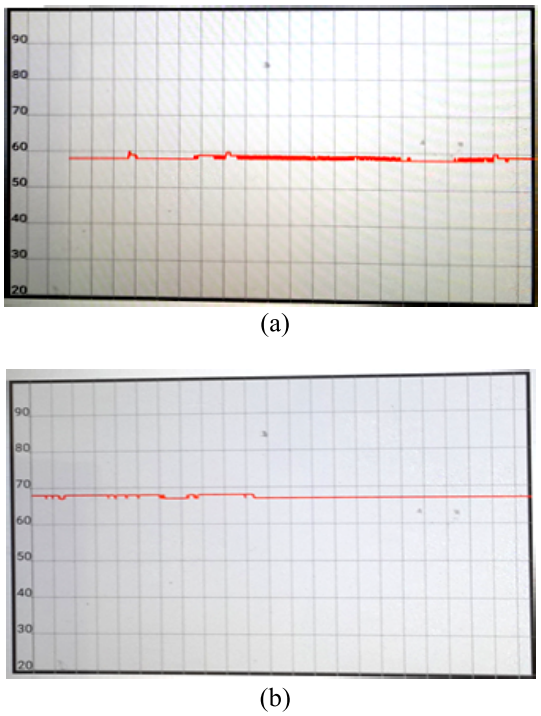

FIGURE 22. Measured sound noise level in dBs at steady state, (a): the proposed MLCC, (b): the traditional chopper circuit.

their associated mechanical vibration and acoustic noise. For implementation of the system in electric vehicles or similar applications, the hardware requires few additional power electronics switching elements, which are cheaper than the solution presented by [7] which, requires changing of the motor design by insertion of copper ring. Also, the proposed MLCC topology is much cheaper in terms of components is compared with the multilevel converter topology presented in [24]. In addition, the new proposed topology has the advantages of reducing voltage stress across switching elements as well as reducing Ohmic losses and electromagnetic interference level due to effective reduction in the current ripples.

VI. CONCLUSION

This paper presents simulation results and experimental validation of a new topology of the multilevel chopper DC/DC converter for a DC motor system. The main objective of the propounded topology is to reduce current ripples and torque ripples that are associated with hard switching of the traditional chopper circuit. The proposed configuration provides constant five values of standard cell voltage and has the ability to generate the required nonstandard voltage within the cell voltage ranges. The generated voltage pattern of this topology has relatively smaller switching ripples compared to the traditional step-down DC/DC power converters. It has been shown that the operation of the DC motor with the new proposed chopper topology can efficiently decrease the motor armature current ripples and torque ripples by a factor equal to the number of the connected voltage cells. As compared with the operation of the motor with traditional chopper circuit, the presented results prove that the mechanical vibration and acoustic noises is reduced by 13 dBs when continuous variable input voltage pattern is applied to the motor and reduced by 8 dBs when steady-state input voltage pattern is applied to the motor.

REFERENCES

[1] D. Sha, J. Zhang, X. Wang, and W. Yuan, "Dynamic response improvements of parallel-connected bidirectional DC–DC converters for electrical drive powered by low-voltage battery employing optimized feedforward control," *IEEE Trans. Power Electron.*, vol. 32, no. 9, pp. 7783–7794, Oct. 2017.

[2] F. Crescimbini, A. Lidozzi, G. L. Calzo, and L. Solero, "High-speed electric drive for exhaust gas energy recovery applications," *IEEE Trans. Ind. Electron.*, vol. 61, no. 6, pp. 2998–3011, Jun. 2014.

[3] A. Adam, A. Elnady, and A. Ghias, "A novel multilevel DC chopper supplying DC motor," in *Proc. 5th Int. Conf. Electron. Devices, Syst. Appl. (ICEDSA)*, Ras al Khaimah, United Arab Emirates, Dec. 2016, pp. 1–5.

[4] R. Silva-Ortigoza, V. M. Hernandez-Guzman, M. Antonio-Cruz, and D. Munoz-Carrillo, "DC/DC buck power converter as a smooth starter for a DC motor based on a hierarchical control," *IEEE Trans. Power Electron.*, vol. 30, no. 2, pp. 1076–1084, Feb. 2015.

[5] M. A. Ahmad, R. M. T. Raja Ismail, and M. S. Ramli, "Control strategy of buck converter driven DC motor: A comparative assessment," *Austral. J. Basic Appl. Sci.*, vol. 4, no. 10, pp. 4893–4903, 2010.

[6] F. Antritter, P. Maurer, and J. Reger, "Flatness based control of a buck-converter driven DC motor," in *Proc. 4th IFAC Symp. Mechatronics Syst.*, Heidelberg, Germany, 2006, pp. 36–41.

[7] J. Hong, S. Wang, Y. Sun, and H. Cao, "An effective method with copper ring for vibration reduction in permanent magnet brush DC motors," *IEEE Trans. Magn.*, vol. 54, no. 11, Nov. 2018, Art. no. 8108105.

[8] D. Torregrossa, A. Khoobroo, and B. Fahimi, "Prediction of acoustic noise and torque pulsation in PM synchronous machines with static eccentricity and partial demagnetization using field reconstruction method," *IEEE Trans. Ind. Electron.*, vol. 59, no. 2, pp. 934–944, Feb. 2012.

[9] G. He, Z. Huang, R. Qin, and D. Chen, "Numerical prediction of electromagnetic vibration and noise of permanent-magnet direct current commutator motors with rotor eccentricities and glue effects," *IEEE Trans. Magn.*, vol. 48, no. 5, pp. 1924–1931, May 2012.

[10] M. Furlan, A. Cernigoj, and M. Boltezar, "A coupled electromagnetic-mechanical-acoustic model of a DC electric motor," *COMPEL-Int. J. Comput. Math. Elect. Electron. Eng.*, vol. 22, no. 4, pp. 1155–1165, 2003.

[11] H. Guhuan, Z. Huang, and D. Chen, "Two-dimensional field analysis on electromagnetic vibration-and-noise sources in permanent-magnet direct current commutator motors," *IEEE Trans. Magn.*, vol. 47, no. 4, pp. 787–794, Apr. 2011.

[12] J. Le Besnerais, V. Lanfranchi, M. Hecquet, and P. Brochet, "Characterization and reduction of audible magnetic noise due to PWM supply in induction machines," *IEEE Trans. Ind. Electron.*, vol. 57, no. 4, pp. 1288–1295, Apr. 2010.

[13] H. Chu, B. Gao, W. Gu, and H. Chen, "Low-speed control for permanent-magnet DC torque motor using observer-based nonlinear triple-step controller," *IEEE Trans. Ind. Electron.*, vol. 64, no. 4, pp. 3286–3296, Apr. 2017.

[14] M. Marchesoni and C. Vacca, "New DC–DC converter for energy storage system interfacing in fuel cell hybrid electric vehicles," *IEEE Trans. Power Electron.*, vol. 15, no. 1, pp. 301–308, Jan. 2007.

[15] J. Linares-Flores, J. Reger, and H. Sira-Ramírez, "Load torque estimation and passivity-based control of a boost-converter/DC-motor combination," *IEEE Trans. Control Syst. Technol.*, vol. 18, no. 6, pp. 1398–1405, Nov. 2010.

[16] H. Sira-Ramírez and M. A. Oliver-Salazar, "On the robust control of buck-converter DC-motor combinations," *IEEE Trans. Power Electron.*, vol. 28, no. 8, pp. 3912–3922, Aug. 2013.

[17] J. Linares-Flores and H. Sira-Ramirez, "A smooth starter for a DC machine: A flatness based approach," in *Proc. 1st Int. Conf. Elect. Electron. Eng.*, Acapulco, Mexico, Sep. 2004, pp. 589–594.

[18] R. Silva-Ortigoza *et al.*, "Two-stage control design of a buck converter/DC motor system without velocity measurements via a-modulator," *Math. Problems Eng.*, vol. 2013, Apr. 2013, Art. no. 929316.
[19] V. M. Hernández-Guzman, R. Silva-Ortigoza, and D. Muñoz-Carrillo, "Velocity control of a brushed DC-motor driven by a DC to DC buck power converter," *Int. J. Innov. Comput., Inf. Control*, vol. 11, no. 2, pp. 509–521, 2015.
[20] G. R. Gerasimos, "Adaptive fuzzy control of DC motors using state and output feedback," *Electr. Power Syst. Res.*, vol. 79, no. 11, pp. 1579–1592, 2009.
[21] Z. Kovacic, M. Balenovic, and S. Bogdan, "Sensitivity-based self-learning fuzzy logic control for a servo system," *IEEE Control Syst.*, vol. 18, no. 3, pp. 41–51, Jun. 1998.
[22] Y. Jianyong, Z. Jiao, and D. Ma, "Adaptive robust control of DC motors with extended state observer," *IEEE Trans. Ind. Electron.*, vol. 61, no. 7, pp. 3630–3637, Jul. 2014.
[23] E. Hernández-Márquez, R. Silva-Ortigoza, J. R. García-Sánchez, M. Marcelino-Aranda, and G. Saldaña-Gonzdlez, "A DC/DC buck-boost converter–inverter–DC motor system: Sensorless passivity-based control," *IEEE Access*, vol. 6, pp. 31486–31492, Jun. 2018. doi: 10.1109/ACCESS.2018.2846614.
[24] V. D. Yurkevich, G. S. Zinoviev, and A. A. Gordeev, "DC motor speed control for electric locomotive equipped by multi-level DC-DC converter," in *Proc. 13th Int. Conf. Seminar Micro/Nanotechnol. Electron. (EDM)*, Jul. 2012, pp. 358–364.
[25] H. Akagi, "Multilevel converters: Fundamental circuits and systems," *Proc. IEEE*, vol. 105, no. 11, pp. 2048–2065, Nov. 2017.

ALI AHMED ADAM ISMAIL received the B.Sc. degree in electrical engineering from the University of Khartoum, Khartoum, Sudan, in 1991, the M.Sc. degree from Bagdad University, Iraq, in 1997, and the Ph.D. degree in electrical engineering from the Technical University of Yildiz, Istanbul, Turkey, in 2007. From 1991 to 2009, he was with the Faculty of Engineering Science, Omdurman Islamic University, Sudan. Until 2013, he was as a Staff Member with Fatih University. Since 2013, he has been an Assistant Professor with the University of Sharjah, Sharjah, United Arab Emirates. His current research interests include control of electrical machines, power electronics applications, propagation of low frequency electromagnetic wave, and microcontroller-impeded systems, and active and passive filters.

A. ELNADY graduated from Cairo University, Cairo, Egypt, in 1990, where he received the master's degree, in 1998 and the Ph.D. degree from the University of Waterloo, Waterloo, ON, Canada, in 2004. His research interests include power-electronics applications in power systems, power quality in distribution systems, smart grids, and integration of renewable sources within power grids.